

---

# Contrastive Counterfactual Visual Explanations With Overdetermination

---

Adam White\*, Kwun Ho Ngan\*  
 James Phelan, Saman Sadeghi Afgeh, Kevin Ryan  
 Constantino Carlos Reyes-Aldasoro, Artur d'Avila Garcez  
 School of Mathematics, Computer Science and Engineering  
 City, University of London, London, EC1V 0HB, UK  
 {Adam.White, Kwun-Ho.Ngan, James.Phelan,  
 Saman.Sadeghiafgeh, Kevin.Ryan,  
 Constantino-Carlos.Reyes-Aldasoro, A.Garcez }@city.ac.uk

## Abstract

A novel explainable AI method called *CLEAR Image* is introduced in this paper. *CLEAR Image* is based on the view that a satisfactory explanation should be contrastive, counterfactual and measurable. *CLEAR Image* explains an image's classification probability by contrasting the image with a corresponding image generated automatically via adversarial learning. This enables both salient segmentation and perturbations that faithfully determine each segment's importance. *CLEAR Image* was successfully applied to a medical imaging case study where it outperformed methods such as Grad-CAM and LIME by an average of 27% using a novel pointing game metric. *CLEAR Image* excels in identifying cases of 'causal overdetermination' where there are multiple patches in an image, any one of which is sufficient by itself to cause the classification probability to be close to one.

## 1 Introduction

AI for Computer Vision can achieve high levels of predictive accuracy, yet the rationale behind these predictions is often opaque. This paper proposes a novel explainable AI (XAI) method called *CLEAR Image* that illuminates the causal structure implicitly modelled by an AI system, where the causes are an image's segments and the effect is the AI system's classification probability. *CLEAR Image* is based on the philosopher James Woodward's seminal analysis of causal explanation [24], which develops Judea Pearl's manipulationist account of causation [14]. We argue that a successful explanation for an AI system should be contrastive, counterfactual and measurable.

According to Woodward, a successful explanation of an event  $E$  must show patterns of counterfactual dependence. This means that it should answer a set of 'what-if-things-had-been-different?' questions, which specify how the event  $E$  would change if, counter to the facts, input conditions had been different. It is only in this way that a user can understand the relevance of different features, and understand the different ways in which changes to the features may affect the outcome. Central to Woodward's account is the requirement for an explanatory equation that relates  $E$  to its causes.

A contrastive explanation seeks to answer the question 'Why  $E$  rather than  $F$ ?'  $F$  is referred to as  $E$ 's foil and it comes from a contrast class of events that were alternatives to  $E$ , but which did not happen [21]. An explanation can thereby identify the causes that led to  $E$  occurring rather than  $F$ , even though the relevant contrast class to which  $F$  belongs is often not explicitly conveyed.

---

\*lead authors

For Woodward, all causal claims are counterfactual and contrastive: ‘to causally explain an outcome is always to explain why it, rather than some alternative, occurred’. In XAI research, counterfactuals usually state minimal changes needed to achieve the desired foil  $F$ .

The ‘causal overdetermination’ of an event occurs when two or more sufficient causes of this event happen. A standard example from the philosophy literature is about the soldiers in a firing squad simultaneously shooting a prisoner, with each shot being sufficient to kill the prisoner. The death of the prisoner is causally overdetermined. This causal structure may well be ubiquitous in learning systems. For example, there may be multiple patches in a medical image, any of which is sufficient in itself to cause a classification probability close to one. To the best of our knowledge, *CLEAR Image* is the first XAI method capable of identifying causal overdetermination.

*CLEAR Image* explains an image’s classification probability by contrasting the image with a corresponding GAN-generated image. This enables the image to be segmented automatically. There follows a process of perturbation, whereby the input values are changed, and the change in outcome is observed to produce a regression equation. The regression equation is then used to determine the contribution each segment makes to the classification probability. *CLEAR Image* identifies counterfactuals and measures the fidelity of its explanation against the classifier.

The contribution of this paper is three-fold. We introduce an XAI method that:

- generates contrastive, counterfactual, measured explanations and can be applied successfully to challenging real-world problems.
- uses a GAN to generate a foil and explicitly explains an image’s classification relative to that foil.
- is capable of identifying causal overdetermination.

*CLEAR Image* was evaluated in two case studies, both involving overdetermination. The first using a multifaceted synthetic dataset, the second using chest X-rays. *CLEAR Image* outperformed XAI methods such as LIME and Grad-CAM by an average of 31% on the synthetic dataset and 27% on the X-ray dataset. Although *CLEAR Image* can be successfully used in any domain, the case studies illustrate its applicability to complex specialist domains such as medical imaging. *CLEAR Image* is a substantial development of an earlier method *CLEAR* (Counterfactual Local Explanations via Regression) which was designed for tabular data [22]. The code for *CLEAR Image* will be made available on GitHub once this paper has been accepted for publication.

## 2 Background

### 2.1 Key Notation

This paper adopts the following notation: let the instance  $x$  be an image, and  $m$  be a machine learning system that maps  $x$  to class label  $l$  with probability  $y$ . Let  $x$  be partitioned into  $S$  segments  $\{s_1, \dots, s_n\}$ . Let any variable with a prime subscript ‘ $'$ ’ be the variable from the GAN-generated image e.g.  $x'$  is the GAN generated image derived from  $x$ , and maps to class  $l$  with probability  $y'$ .

### 2.2 Explanation by Perturbation

Methods such as Occlusion [27], Extremal Perturbation [7], FIDO [3], LIME [15] and Kernel SHAP [11] use perturbation to evaluate which segments (regions) of an image  $x$  are most responsible for  $x$ ’s classification probability  $y$ . The underlying idea is that the contribution that a segment  $s_i$  makes to  $y$  can be determined by substituting it with an uninformative segment  $s'_i$ , where  $s'_i$  may be either grey, black or blurred [27, 7, 15] or in-painted without regard to any contrast class [3]. There are three key problems with using perturbed images to explain a classification:

1. A satisfactory explanation must have a relevant foil  $F$ ; it must answer ‘Why  $E$  rather than  $F$ ?’ However, none of the above methods does this. Their foils are instead images of uninformative segments.
2. The substitution method can fail to identify the contribution  $s_i$  makes to  $y$ . For example, replacing  $s_i$  with a black  $s'_i$  might take the entire image outside of the classifier  $m$ ’s training distribution. By contrast, blurring or uninformative in-painting might result in  $s'_i$  being too similar to  $s_i$  resulting in the contribution of  $s_i$  being underestimated.

3. A segmentation needs to be relevant to its explanatory question. Current XAI perturbation methods produce radically different segmentations. [3, 7] identify ‘optimal’ segments that, when substituted by an uninformative segment, maximally affect the classification probability; by contrast, [15] uses a texture/intensity/colour algorithm (e.g. Quickshift).

CLEAR *Image* uses GAN generated images to address each of these problems: (i) its foil is a GAN generated image  $x'$  belonging to the contrast class  $l'$  selected by the user. (ii) inpainting with segments derived from  $x'$  enables better estimation of each segment’s contribution to the difference between probabilities  $y$  and  $y'$ . (iii) the differences between  $x$  and  $x'$  are used to guide the segmentation.

### 3 Related Work

The XAI methods most relevant to this paper can be broadly grouped into three types:

**Gradient-based methods.** These provide saliency maps by backpropagating an error signal from a neural network’s output to either the input image or an intermediate layer. Simonyan et al. [19] use the derivative of a class score for the image to assign an importance score to each pixel; the saliency maps are however often noisy. Kumar et al.’s CClass-Enhanced Attention Response (CLEAR) [10] uses backpropagation to visualise the most dominant classes; this should not be confused with our method. A second approach modifies the backpropagation algorithm to produce sharper saliency maps, for example, by suppressing the negative flow of gradients; prominent examples of this approach [20, 25] have been found to be invariant to network reparameterization and/or the class predicted [1, 12]. A third approach [17, 4] uses the product of gradients and activations starting from a late layer. In Grad-CAM [17], the product is clamped to only highlight positive influences on class scores.

**Perturbation based methods.** LIME and Kernel SHAP [15, 11] generate a dataset of perturbed images, which feeds into a regression model, which then calculates segment importance scores [15] or Shapley Values [11]. These bear some similarity to CLEAR *Image* but key differences include: they do not use a GAN generated image, do not identify counterfactuals and do not report their fidelity. Extremal Perturbation [7] uses gradient descent to determine an optimal perturbed version of an image that, for a fixed area, has the maximal effect on a network’s output whilst guaranteeing that the selected segments are smooth. Chang et al. [3] use variational Bernoulli drop to find a minimal set of segments that would change an image’s class. In contrast to [11, 15, 7], this method uses a GAN to in-paint segments with ‘plausible alternative values’, however, these values are not generated so as to belong to a chosen contrast class. Furthermore, segment importance scores are not generated.

**GAN difference methods.** Generative adversarial network (GAN) [8] has been widely applied for synthetic image generation. Image translation through direct mapping of the original image to its target classes has gained popularity, such as CycleGAN [28] and StarGAN [6]. StarGAN V2 [5] introduced a style vector for conditional image translation and produced high quality images over a diverse set of target conditions. These models, however, do not keep the translation minimal and make modification even for intra-domain translation. Fixed-point GAN [18] introduced an identity loss penalizing any deviation of the image during intra-domain translation. This aims to enhance visual similarity with the original image. DeScarGAN [23] adopts this loss function in its own GAN architecture and has outperformed Fixed-point GAN in their case study for Chest X-Ray pathology identification and localisation.

CLEAR *Image* builds on the strengths of these methods but also addresses key shortcomings. Subtracting a GAN-generated image from an original image is often insufficient for explaining a classification probability, as the segments highlighted by this approach can vary significantly in their relevance. CLEAR *Image*, therefore, provides importance scores for each segment. CLEAR *Image* also takes into account that counterfactuals by themselves provide incomplete explanations. There needs to be an equation specifying the entire causal relationship between the segments and the classification probability. Next, methods such as LIME assume that a classification probability is a simple linear addition of its causes. This is incorrect for cases of causal overdetermination, and CLEAR *Image* therefore uses a sigmoid function. Finally, prominent XAI methods often fail to identify the most relevant regions of an image, CLEAR *Image* therefore measures the fidelity of its explanations.

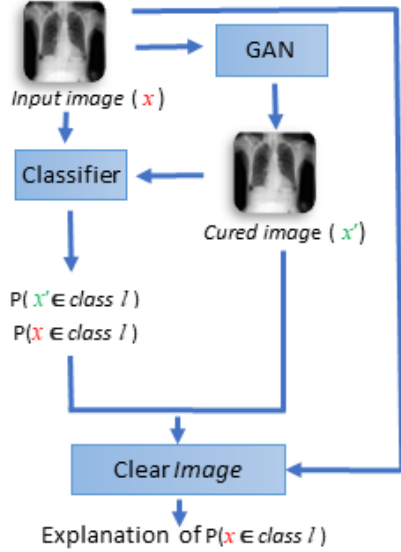
## 4 The CLEAR *Image* Method

CLEAR *Image* is a model-agnostic XAI method that explains the classification of an image made by any classifier. It requires both image  $x$  and a contrast image  $x'$ , usually generated by a GAN. CLEAR *Image* segments  $x$  into  $\{s_1, \dots, s_n\} \in S$  and then applies the same segmentation to  $x'$  creating  $\{s'_1, \dots, s'_n\} \in S'$ . CLEAR *Image* determines the contributions that different subsets of  $S$  make to  $y$  by substituting with the corresponding segments of  $S'$ . CLEAR *Image* is GAN agnostic, allowing the user to choose the GAN architecture most suitable to their project. A set of ‘image-counterfactuals’  $\{c_1 \dots c_k\}$  is also identified.

**Definition 4.1** An **image-counterfactual**  $c_j$  from  $l$  to  $l'$  is an image resulting from a change in the values of one or more segments of  $x$  to their corresponding values in  $S'$  such that  $\text{class}(m(x)) = l$ ,  $\text{class}(m(c_j)) = l'$  and  $l \neq l'$ . The change is minimal in that if any of the changed segments had remained at its original value, then  $\text{class}(m(x)) = \text{class}(m(c_j))$ .

CLEAR *Image* uses a regression equation to quantify the contribution that individual segments make to  $y$ . It then measures the fidelity of its regression by comparing the classification probability resulting from each  $c_j$  with an estimate of that change calculated from the regression equation.

**Definition 4.2** **counterfactual-regression fidelity error** =  $|\text{regression equation}(c_j) - y_{c_j}|$




---

### Algorithm 1: CLEAR *Image*

---

**input** :  $x$  - diseased image,  
 $x'$  - contrast image  
 $m$  - AI classifier  
 $S, S' \leftarrow \text{Segment\_Images}(x, x')$   
 $D \leftarrow \text{Create\_Synthetic\_Data}(S, S', m)$   
 $C \leftarrow \text{Find\_Counterfactuals}(m, S, S')$   
 $r \leftarrow \text{Find\_Regression\_Equation}(D, C)$   
 $O \leftarrow \text{Find\_Overdetermination}(r)$   
 $G \leftarrow \text{Calculate\_Segment\_Scores}(r)$   
 $C_r \leftarrow \text{Estimate\_Counterfactual\_Probs}(r, C)$   
 $e \leftarrow \text{Calculate\_Fidelity}(C, C_r)$   
**return**  $\text{expl} = \langle G, C, C_r, r, O, e \rangle$

---

Figure 1: The CLEAR *Image* pipeline.

The following steps generate an explanation of prediction  $y$  for image  $x$ :

1. Segment image. There are 2 options: (a) Thresholding. The segmentation is solely determined by applying a user-defined threshold to the difference mask between  $x$  and  $x'$ . (b) Thresholding & Felzenszwalb. The segmentation from the first option is supplemented by applying a 2nd lower threshold to the unsegmented regions of the difference mask and then applying a combination of connected component labelling, erosion and the Felzenszwalb algorithm.
2. Determine  $x$ 's image-counterfactuals. A dataset of perturbed images is created by selectively replacing segments of  $x$  with the corresponding segments of  $x'$ . A separate image is created for every combination in which either 1, 2, 3, or 4 segments are replaced. Each perturbed image is then passed through  $m$  to determine its classification probability. All image-counterfactuals involving changes in up to 4 segments are then identified.
3. Generate a regression dataset of perturbed images. Perturbed images are created by randomly replacing segments of  $x$  with the corresponding segments of  $x'$ , and their classification probabilities are then determined by  $m$ . These are added to the dataset created in step 2. If necessary, a simple genetic algorithm is then used to generate additional images around the decision boundary.

4. Perform a stepwise logistics regression. This is carried out using a binary representation of each segment of each image in the regression dataset. Each segment  $s$  that is from  $x$  is represented by a 1, and each segment  $s'$  from  $x'$  is represented by a 0. The observations corresponding to image-counterfactuals (from step 2) are given a high weighting and act as soft constraints on the subsequent regression.
5. Measure the fidelity of the regression by calculating fidelity errors (see Figure 3) and goodness of fit statistics.
6. Iterate to best explanation. Because CLEAR *Image* produces fidelity statistics, its parameters can be iteratively changed to achieve a better trade-off between interpretability and fidelity. Key parameters include segmentation type and number of segments to include in regression.
7. Calculate segment importance scores. These are the regression coefficients for each segment.

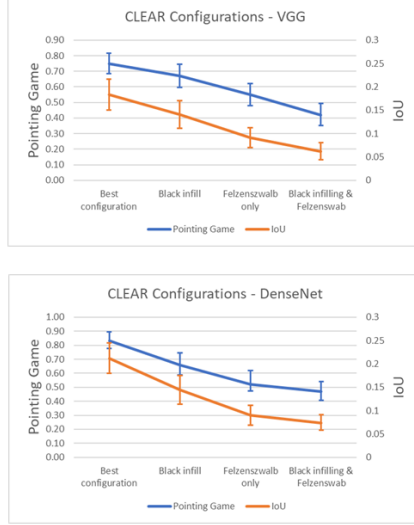


Figure 2: Evaluation metrics (with 95% confidence intervals) for different configurations of CLEAR with CheXpert dataset.

---

#### Algorithm 2: Pointing Game

---

```

input :  $x$  - diseased image,  $A$  - annotated
         features
          $w$  - XAI saliency map
 $P_A \leftarrow$  Square_Idx_of_Each_Feature( $A, x$ )
 $Q \leftarrow$  Average_Intensity_Each_Square( $w$ )
 $Q' \leftarrow$  Square_Idx_Sort_Highest_Intensity( $Q$ )
 $hits \leftarrow 0$ ;  $misses \leftarrow 0$ ;  $h_A \leftarrow False$ 
foreach  $q'_i \in Q'$  do
    // starting with highest
    foreach  $a_j \in A$  do
        if  $q'_i \in P_{a_j}$  then // square idx
            match
            |  $hits \leftarrow hits + 1$ ;  $h_{a_j} \leftarrow True$ 
        else
            |  $misses \leftarrow misses + 1$ 
    if  $\forall a_j (h_{a_j} = True)$  then
        // exit once all features hit
        | break
return  $\langle hits, misses \rangle$ 

```

---

For CLEAR *Image* an explanation (expl) is a tuple  $\langle G; C; C_r; r; O, e \rangle$ , where  $G$  are segment importance scores,  $C$  and  $C_r$  are image-counterfactuals (actual and estimated),  $r$  is a regression equation,  $O$  are the causes resulting in overdetermination, and  $e$  are fidelity errors. Figure 3 shows extracts from a CLEAR *Image* report.

The causal overdetermination of an effect occurs when multiple sufficient causes of that effect occur. By default, CLEAR *Image* only reports sufficient causes which each consist of a single segment belonging to  $S$ . Substituting a sufficient cause with its corresponding member in  $S'$  guarantees the effect. In philosophy of science, it is generally taken that for an effect to be classified as overdetermined, it should be narrowly defined, such that all the sufficient causes have the same, or very nearly the same impact [13]. For the case studies, the effect is defined as  $p(x \in \text{diseased}) > 0.99$ , though the user may choose a different probability threshold. A sufficient cause changes a GAN generated healthy image to a diseased image. This is in the opposite direction to CLEAR *Image*'s counterfactuals which 'cure' a diseased image. Sufficient causes can be read off from CLEAR *Image*'s regression equation. Using the example in Figure 3 with the logistic formula, a classification probability of  $> 0.99$  requires  $\mathbf{w}^T \mathbf{x} > 4.6$ . The GAN healthy image corresponds to all the binary segment variables being equal to zero. Hence,  $\mathbf{w}^T \mathbf{x}$  is equal to the intercept value of -4.9, giving a probability of  $(1 + \exp^{4.9})^{-1} \approx 0.01$ . If a segment  $s'_i$  is now replaced by  $s_i$ , the corresponding binary variable changes to 1. Hence if segment 9 is infilled, then  $Seg09 = 1$  and  $\mathbf{w}^T \mathbf{x} = 6.8$  (i.e.  $11.7 - 4.9$ ). Similarly, infilling just segment 11 will make  $\mathbf{w}^T \mathbf{x} > 4.6$ . Either substitution is sufficient to guarantee  $\mathbf{w}^T \mathbf{x} > 4.6$ , irrespective of any other changes that could be made to the values of the other segment variables. Hence segments 9 & 11 are each a sufficient cause and there is overdetermination.

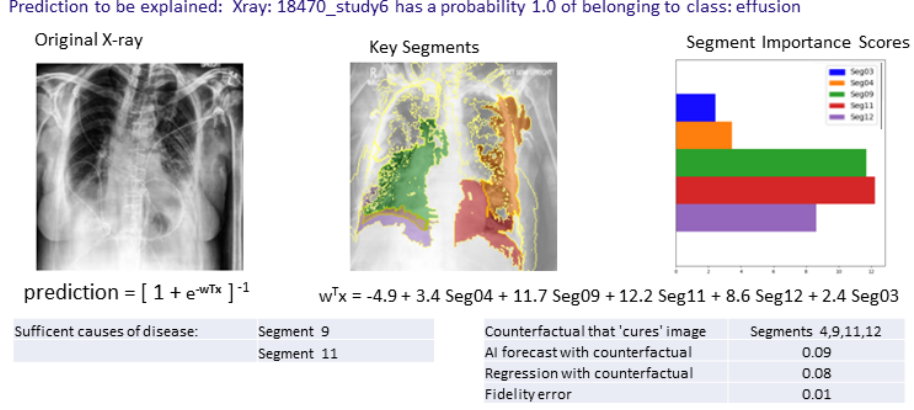


Figure 3: Extracts from a CLEAR *Image* report. The report states that the segments 4,9,11 & 12 all need to be infilled to flip the classification of the X-ray to ‘healthy’. According to CLEAR’s logistic regression equation infilling these segments changes the probability of the X-ray being classified as ‘effusion’ to 0.08. However when these segments were actually infilled and passed through the classifier, the probability changed to 0.09, hence the fidelity error is 0.01. CLEAR *Image* also identifies that segments 9 and 11 are each sufficient causes of the X-ray being diseased.

## 5 Experimental Investigation

There are two case studies, the first using a synthetic dataset, the second analysing pleural effusion X-rays taken from the CheXpert dataset [9]. Transfer learning was used to train both a VGG-16 with batch normalization and a DenseNet-121 classifier for each dataset. CLEAR *Image* was evaluated against Grad-CAM, Extremal Perturbations and LIME. The evaluation consisted of both a qualitative comparison of saliency maps and a comparison of pointing game and intersection over union scores. CLEAR *Image*’s fidelity errors were also analysed (none of the other XAI methods measures fidelity).

### 5.1 Datasets

The synthetic dataset’s images share some key characteristics found in medical imaging including: (i) different combinations of features leading to the same classification (ii) irrelevant features. All images (healthy and diseased) contain: a set of concentric circles, a large and a small ellipse. An image is ‘diseased’ if either: (1) the small ellipse is thin-lined, and the large ellipse contains a square or (2) there is a triangle, and the large ellipse contains a square. The dataset is adapted from [23].

CheXpert is a dataset of Lung X-Ray with automated pathological label extraction through radiology reports, consisting of 224,316 radiographs of 65,240 patients in total [9]. Images were extracted just for the classes ‘pleural effusion’ and ‘no finding’. Mis-classified images and images significantly obstructed by supporting devices were manually filtered. A random frontal X-ray image per patient was collected. In total, a dataset of 2,440 images was used in this work for model training, validation and testing. Appendix A details of the data preparation process. A hospital doctor provided the ground truth annotation to 125 X-ray images with pleural effusion for our case study.

### 5.2 GAN-Based Image Generation

To generate contrastive images, DeScarGAN [23] and StarGAN-V2 [5] have been deployed as the network architectures for the synthetic dataset and the CheXpert dataset respectively. The use of these established GAN networks demonstrates how the generated contrastive images can aid in the overall CLEAR *Image* pipeline. Default training hyperparameters were applied unless otherwise stated. Details of model training and hyperparameters can be found in Appendix B. The source image was applied as input for the Style Encoder instead of a specific reference image for StarGAN-V2. This ensures the generated style mimics that of the input source images. StarGAN-V2 is also not locally constrained (i.e. the network will modify all pixels in an image related to the targeted class which will include irrelevant spurious regions of the image). A post generation lung space segmentation step using a pre-trained U-Net model was implemented and the original diseased lung space is replaced

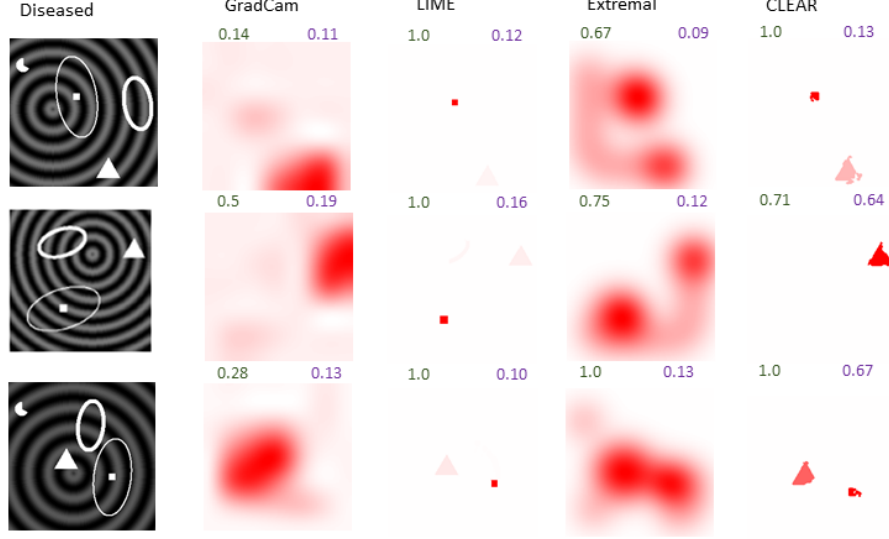


Figure 4: Comparison of XAI methods on synthetic data. The pointing game scores are shown in green and the IoU scores are in purple. The significance of a patch is indicated by its red intensity.

with the generated image with a Gaussian Blur process to fuse the edge effect as shown in Figure 5. This reduces the feature identification space within the lung space.

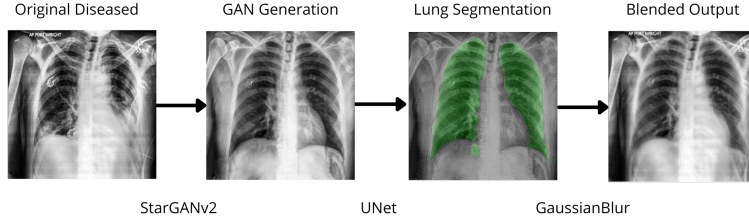


Figure 5: The post-processing pipeline for GAN generated image.

### 5.3 Evaluation Metrics

This paper uses two complementary metrics to evaluate XAI methods. Both require annotated images identifying ‘target’ regions that should be critical to their classification. A pointing game produces the first metric, which measures how successfully a saliency map ‘hits’ an image’s targets. Previously pointing games have been designed for cases where (i) images have single targets (ii) the saliency maps have a maximum intensity point [7, 26]. By contrast, this paper’s case studies have multiple targets, and the pixels within each CLEAR *Image* segment have the same value. We, therefore, formulated a novel pointing game. The pointing game partitions a ‘diseased’ image into 49 square segments,  $P = \{p_1 \dots p_{49}\}$  and identifies which squares contain each of the targets. The corresponding saliency map is also partitioned, and each square is allocated a score equal to the average intensity of that square’s pixels  $Q = \{q_1 \dots q_{49}\}$ . The pointing game then starts with the  $q_i$  of highest intensity and determines if the corresponding  $p_i$  contains a relevant feature. A successful match is a ‘hit’ and an unsuccessful match is a ‘miss’. This process continues until every target has at least one hit. The score for an image is the number of hits over the number of hits plus misses. Pseudocode is provided in Algorithm 2.

The second metric is intersection over union (henceforth: IoU). In order to apply IoU each pixel in a saliency map is classified as being ‘salient’ if it is above the 70<sup>th</sup> percentile of intensities in that map. IoU then measures the overlap between the ‘salient’ pixels  $pix^{salient}$  and the pixels belonging to the image’s targets  $pix^{target}$ :  $IOU = (pix^{salient} \cap pix^{target}) / (pix^{salient} \cup pix^{target})$ .

Both metrics are useful but have counterexamples. For example, IoU would give too high a score to a saliency map that strongly overlapped with a large image target but completely missed several



smaller targets that were also important to a classification. However, applied together, the two metrics provide a good indication of an XAI’s performance.

## 5.4 Experimental Runs

*CLEAR Image* was run using logistic regression with the Akaike information criterion. The segmentation algorithms used were ‘Thresholding’ for the synthetic dataset and ‘Thresholding & Felzenszwalb’ for CheXpert. The average running time for *CLEAR Image* was 20 seconds per image for the synthetic dataset and 38 seconds per image for the CheXpert dataset, running on a Windows i7-8700 RTX 2070 PC. Default parameter values were used for the other XAI methods, except for the following beneficial changes: Extremal Perturbations was run with ‘fade to black’ perturbation type, and using areas {0.025,0.05,0.1,0.2} with the masks summed and a Gaussian filter applied. LIME was run using Quickshift segmentation with kernel sizes 4 and 20 for CheXpert and synthetic dataset respectively.

## 5.5 Experimental Results

*CLEAR Image* outperforms the other XAI methods on both datasets (Figure 6). Furthermore, its fidelity errors are low, indicating that the regression coefficients for the counterfactually important segments are accurate. Figure 2 illustrates some of the benefits of using GAN generated images for: (i) segmentation compared with using the Felzenszwalb algorithm (ii) inpainting compared with using black patches. *CLEAR Image*’s performance was mostly very similar for the VGG-16 and DenseNet. Therefore, only the DenseNet results will be presented unless otherwise stated.

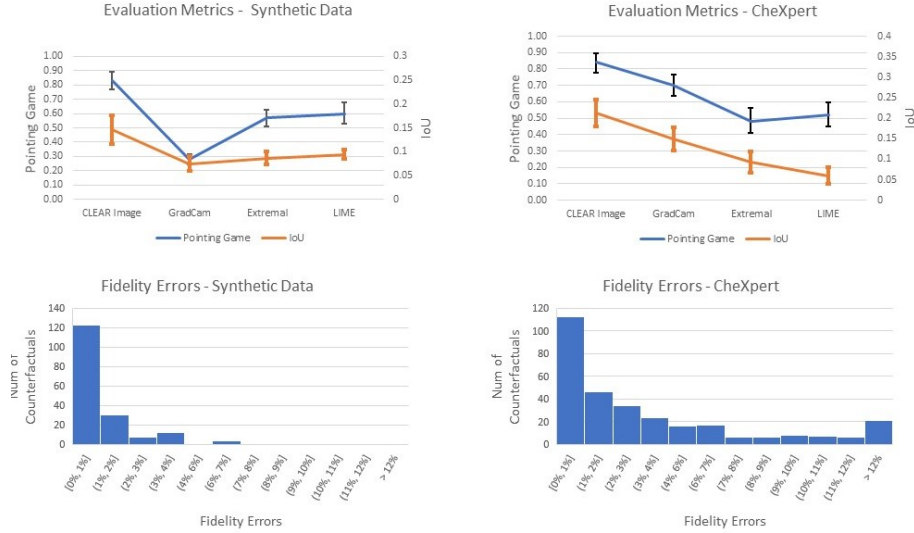


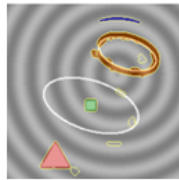
Figure 6: Evaluation metrics (with 95% confidence intervals) and fidelity errors for DenseNet models

Prediction to be explained: Synthetic Image has a probability 1.0 of belonging to class: diseased

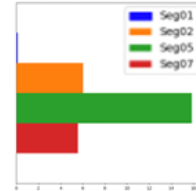
Original X-ray



Key Segments



Segment Importance Scores



$$\text{prediction} = [1 + e^{-w^T x}]^{-1}$$

$$w^T x = -16.8 + 16.0 \text{ Seg05} + 6.0 \text{ Seg02} + 5.6 \text{ Seg07} + 0.1 \text{ Seg01}$$

Figure 7: Extracts from a *CLEAR Image* report for a synthetic image. The regression equation shows that Seg05 is a necessary but insufficient cause of the X-ray being diseased.



CLEAR *Image*’s regression equation was able to capture the relatively complex causal structure that generated the synthetic dataset. A square (SQ) is a *necessary but insufficient* cause for being diseased. An image is labelled as diseased if there is also either a triangle (TR) or the small ellipse is thin-lined (TE). When SQ, TR and TE are all present in a single image, there is a type of overdetermination in which TR and TE are each a sufficient cause *relative* to the ‘image with SQ already present’. Figure 7 shows an example. As before, a healthy image corresponds to the binary segment variables equalling one and a classification probability of  $>0.99$  requires  $w^T x > 4.6$ . This can only be achieved by Seg 5 (corresponding to SQ) plus at least one of Seg 2 or Seg 7 (TE, TR) being set to 1 (i.e. being present).

For the CheXpert dataset, a qualitative assessment of the segments show that CLEAR *Image* allows for a greater appreciation of the pathology compared to ‘broad-brush’ methods such as Grad-CAM. Nevertheless, the segmentation can be further improved based on the IoU scores. For CheXpert’s counterfactuals, only 5% of images did not have a counterfactual with four or fewer  $s'$  segments. Most images required several  $s'$  segments to be infilled before its classification flipped to ‘cured’, 17% required one segment, 30% with two segments, 24% with three segments and 24% with four segments. 17% of the X-rays were found to be causally overdetermined.

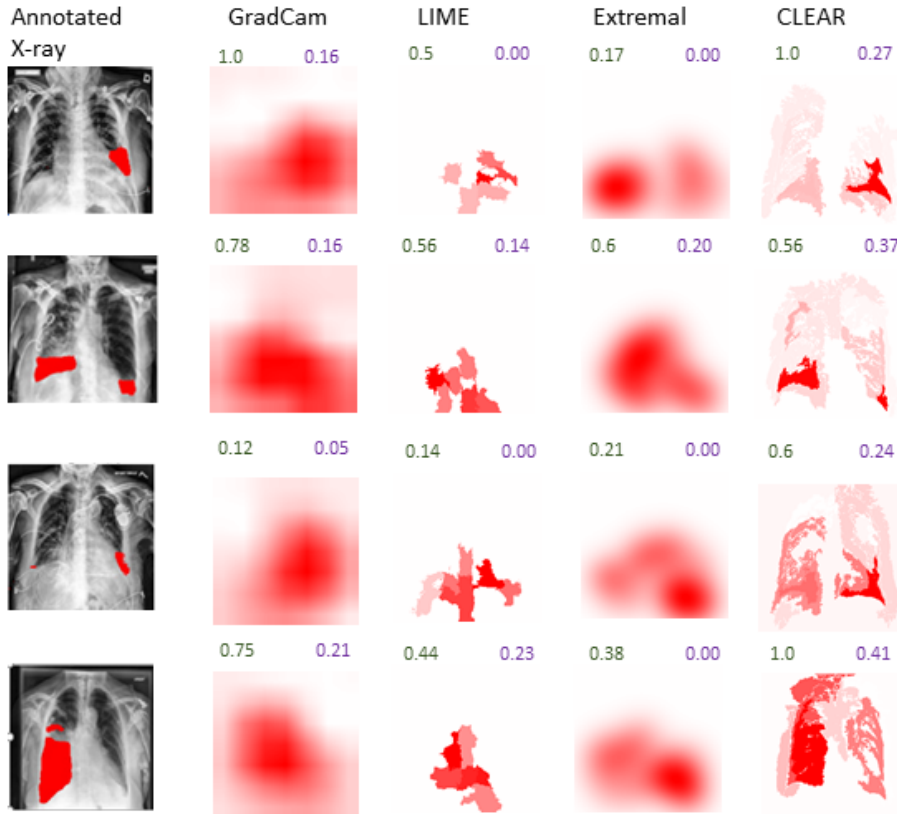


Figure 8: Comparison of XAI methods on X-ray. The pointing game scores are shown in green and the IoU scores are in purple. The significance of a patch is indicated by its red intensity.

## 6 Discussion

As AI systems for image data are increasingly adopted in society, understanding their implicit causal structures has become paramount. Yet the explanations provided by XAI methods cannot always be trusted, as the differences in Figure 8’s saliency maps illustrate. It is therefore critical that an XAI method measures its own fidelity. By ‘knowing when it does not know’, it can alert the user when its explanations are unfaithful. By providing explanations that can be trusted, CLEAR *Image* has the potential to have a large positive impact on a wide-range of applications of AI for Computer Vision. Its intended use of GANs (e.g. in the explanation of medical imaging) appears to have minimal potential for negative societal impact. Any undesired risks can be mitigated by ensuring that the GAN

image used as a foil is always shown and there is complete transparency of the data and process used in generating that image.

A key limitation of *CLEAR Image* is that it first requires training a GAN, and this can be a challenging and time-consuming process. Another possible limitation could be the understandability of *CLEAR Image* to non-technical users. However, its reports can be suitably tailored, for example only showing saliency maps, lists of counterfactuals and cases of overdetermination.

We have shown that *CLEAR Image* can illuminate cases of causal overdetermination. Many other types of causal structure may also be ubiquitous in AI systems. For example, causal pre-emption, double pre-emption and causal clustering are well documented within the philosophy of science [2, 16]. The relevance of these to XAI will be a future area of work. Another area will be improving segmentation, e.g. by introducing domain-specific constraint parameters for GANs, to minimise the modifications of specified attributes (e.g. changes in the heart for lung X-ray image generation).

## References

- [1] Julius Adebayo et al. “Sanity checks for saliency maps”. In: *arXiv preprint arXiv:1810.03292* (2018).
- [2] Michael Baumgartner. “Inferring causal complexity”. In: *Sociological methods & research* 38.1 (2009), pp. 71–101.
- [3] Chun-Hao Chang et al. “Explaining image classifiers by counterfactual generation”. In: *arXiv preprint arXiv:1807.08024* (2018).
- [4] Aditya Chattopadhyay et al. “Grad-cam++: Generalized gradient-based visual explanations for deep convolutional networks”. In: *2018 IEEE Winter Conference on Applications of Computer Vision (WACV)*. IEEE, 2018, pp. 839–847.
- [5] Yunjey Choi et al. “StarGAN v2: Diverse Image Synthesis for Multiple Domains”. In: *2020 IEEE/CVF Conference on Computer Vision and Pattern Recognition (CVPR)*. 2020, pp. 8185–8194. DOI: 10.1109/CVPR42600.2020.00821.
- [6] Yunjey Choi et al. “Stargan: Unified generative adversarial networks for multi-domain image-to-image translation”. In: *Proceedings of the IEEE conference on computer vision and pattern recognition*. 2018, pp. 8789–8797.
- [7] Ruth Fong, Mandela Patrick, and Andrea Vedaldi. “Understanding deep networks via extremal perturbations and smooth masks”. In: *Proceedings of the IEEE/CVF International Conference on Computer Vision*. 2019, pp. 2950–2958.
- [8] Ian Goodfellow et al. “Generative adversarial nets”. In: *Advances in neural information processing systems*. 2014, pp. 2672–2680.
- [9] Jeremy Irvin et al. *CheXpert: A Large Chest Radiograph Dataset with Uncertainty Labels and Expert Comparison*. 2019. arXiv: 1901.07031 [cs.CV].
- [10] Devinder Kumar, Alexander Wong, and Graham W Taylor. “Explaining the unexplained: A class-enhanced attentive response (clear) approach to understanding deep neural networks”. In: *Proceedings of the IEEE Conference on Computer Vision and Pattern Recognition Workshops*. 2017, pp. 36–44.
- [11] Scott M Lundberg and Su-In Lee. “A unified approach to interpreting model predictions”. In: *Advances in Neural Information Processing Systems*. 2017, pp. 4765–4774.
- [12] Weili Nie, Yang Zhang, and Ankit Patel. “A theoretical explanation for perplexing behaviors of backpropagation-based visualizations”. In: *International Conference on Machine Learning*. PMLR. 2018, pp. 3809–3818.
- [13] Laurie Ann Paul. “Counterfactual theories”. In: *The Oxford handbook of causation*. 2009.
- [14] Judea Pearl. *Causality: Models, Reasoning and Inference*. 2nd. New York, NY, USA: Cambridge University Press, 2009.

- [15] Marco Tulio Ribeiro, Sameer Singh, and Carlos Guestrin. “Why Should I Trust You? Explaining the Predictions of Any Classifier”. In: *Proc. ACM SIGKDD 2016. KDD ’16*. San Francisco, California, USA: ACM, 2016, pp. 1135–1144. ISBN: 978-1-4503-4232-2. DOI: 10.1145/2939672.2939778. URL: <http://doi.acm.org/10.1145/2939672.2939778>.
- [16] Jonathan Schaffer. “Trumping preemption”. In: *The Journal of Philosophy* 97.4 (2004), pp. 165–181.
- [17] Ramprasaath R Selvaraju et al. “Grad-cam: Visual explanations from deep networks via gradient-based localization”. In: *Proceedings of the IEEE international conference on computer vision*. 2017, pp. 618–626.
- [18] Md Mahfuzur Rahman Siddiquee et al. “Learning fixed points in generative adversarial networks: From image-to-image translation to disease detection and localization”. In: *Proceedings of the IEEE International Conference on Computer Vision*. 2019, pp. 191–200.
- [19] Karen Simonyan, Andrea Vedaldi, and Andrew Zisserman. “Deep inside convolutional networks: Visualising image classification models and saliency maps”. In: (2014).
- [20] Jost Tobias Springenberg et al. “Striving for simplicity: The all convolutional net”. In: *arXiv preprint arXiv:1412.6806* (2014).
- [21] Bas C Van Fraassen et al. *The scientific image*. Oxford University Press, 1980.
- [22] Adam White and Artur d’Avila Garcez. “Measurable counterfactual local explanations for any classifier”. In: *arXiv preprint arXiv:1908.03020* (2019).
- [23] Julia Wolleb, Robin Sandkühler, and Philippe C Cattin. “DeScarGAN: Disease-Specific Anomaly Detection with Weak Supervision”. In: *International Conference on Medical Image Computing and Computer-Assisted Intervention*. Springer. 2020, pp. 14–24.
- [24] J. Woodward. *Making things happen: a theory of causal explanation*. Oxford, England: Oxford University Press, 2003. ISBN: 9780195189537.
- [25] Matthew D Zeiler and Rob Fergus. “Visualizing and understanding convolutional networks”. In: *European conference on computer vision*. Springer. 2014, pp. 818–833.
- [26] Jianming Zhang et al. “Top-down neural attention by excitation backprop”. In: *International Journal of Computer Vision* 126.10 (2018), pp. 1084–1102.
- [27] Bolei Zhou et al. “Learning deep features for discriminative localization”. In: *Proceedings of the IEEE conference on computer vision and pattern recognition*. 2016, pp. 2921–2929.
- [28] Jun-Yan Zhu et al. “Unpaired image-to-image translation using cycle-consistent adversarial networks”. In: *Proceedings of the IEEE international conference on computer vision*. 2017, pp. 2223–2232.

## A Data Preparation and Sample Results for the CheXpert dataset

### A.1 Data Pre-Processing

CheXpert has a total of 14 pathological observations, including ‘No Finding’ are labelled through an automated rule-based labeller from text radiology reports. For each observation, the Stanford team has classified each radiograph as either negative (0), uncertain (-1) or positive (1). Other metadata includes gender, age, X-ray image projection and presence of supporting devices.

In this study, this dataset (v1.0) was applied for the model development of a binary classification task to demonstrate the capability of CLEAR *Image* as an explainable AI framework. An initial filtering process of the metadata was applied for the two classes used in the study - (1) Diseased with Pleural Effusion and (2) Healthy (This is assumed to be X-ray images with no findings and no positive observations in any of the pathological conditions). To minimise potential complication with other pathological conditions, X-ray images with only positive in pleural effusion were used with other pathological categories either as negative/blank.

A review of the filtered images also identified that the dataset was curated with some images having significant artefacts that can hamper model training performance. Figure 9 presents some of these images in both diseased and healthy categories. Many of them consist of artefacts from image capturing and processing (e.g. image distortion, orientation, low resolutions or miscalibration). Some images were also significantly obstructed by limbs or support devices. Some healthy images were also wrongly labelled according to a hospital doctor. A secondary manual filtering was conducted to remove any identified images with artefacts.

The 2440 selected were split approximately 80/10/10 for the training/validation/testing. The images were also resized to 256 x 256 as the input into the classification model and generative adversarial network (GAN) as described in Section 5. Figure 10 presents some of the typical images in the final dataset for both diseased and healthy categories.

### A.2 Further CheXpert Results

Additional sample results are presented that display the most important segments (regions) identified by each XAI method (Figures 11 & 12). These are the pixels of each saliency map that are above the 70<sup>th</sup> percentile of intensities for that map i.e. the segments used for calculating the IoU scores. Figure 11 is for the DenseNet model and Figure 12 is for the VGG model. These illustrate both the higher precision of CLEAR *Image* compared to the other XAI methods, and the different behaviours of the VGG and DenseNet models.

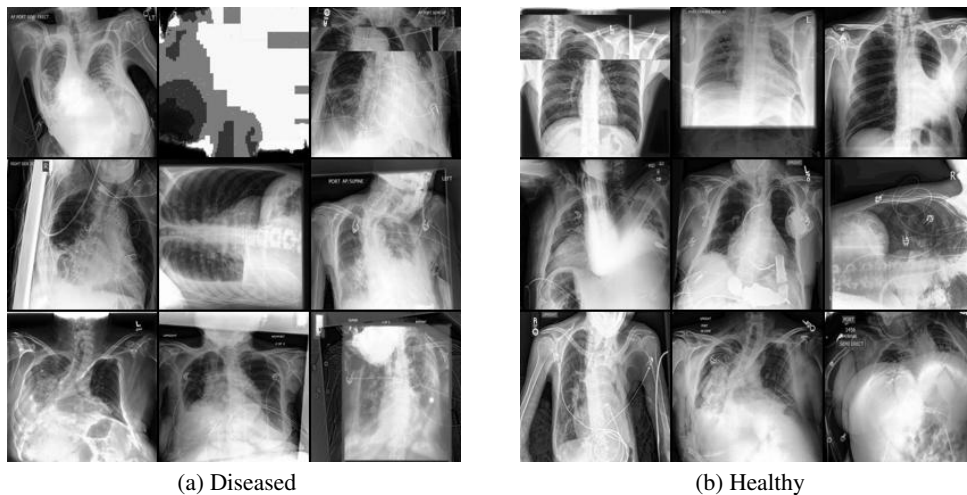


Figure 9: Representative examples of poorly curated images including image distortion, mis-orientation, obstruction by limbs and support devices as well as significant spine deformation.

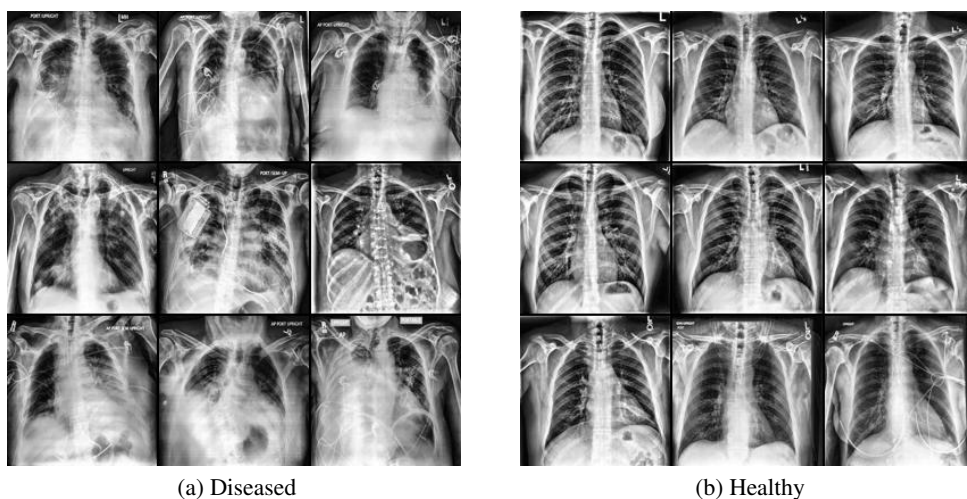


Figure 10: Representative examples of final images for (a) diseased with identifiable regions of pathology and (b) healthy images with clear air space. All images have minimal obstructions from support devices.

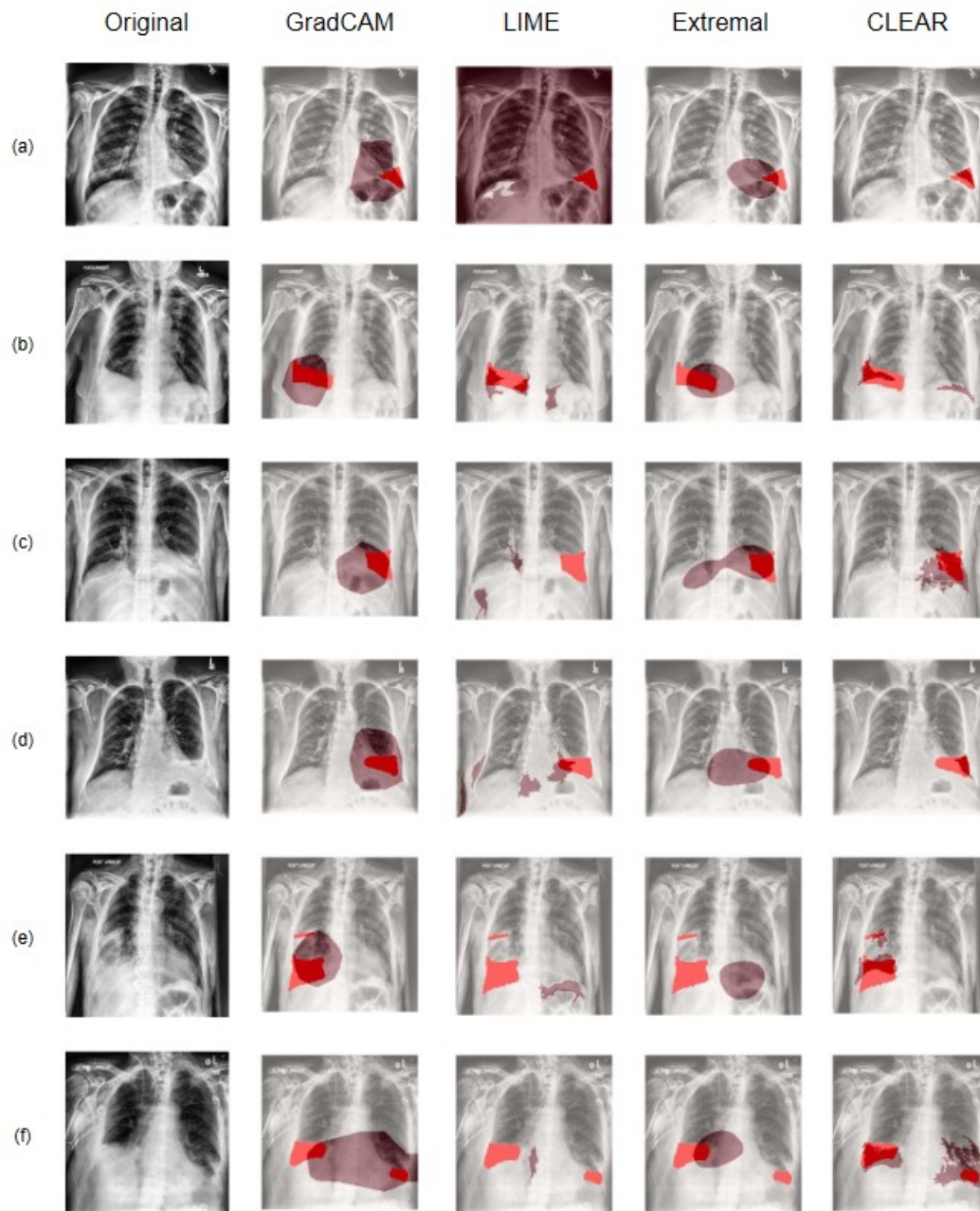


Figure 11: Representative comparative examples of the identified important segments of a DenseNet-based image classification model (Val Acc: 98.8%) for pleural effusion using (i) CLEAR *Image*, (ii) Grad-CAM, (iii) Extremal Perturbation and (iv) LIME.

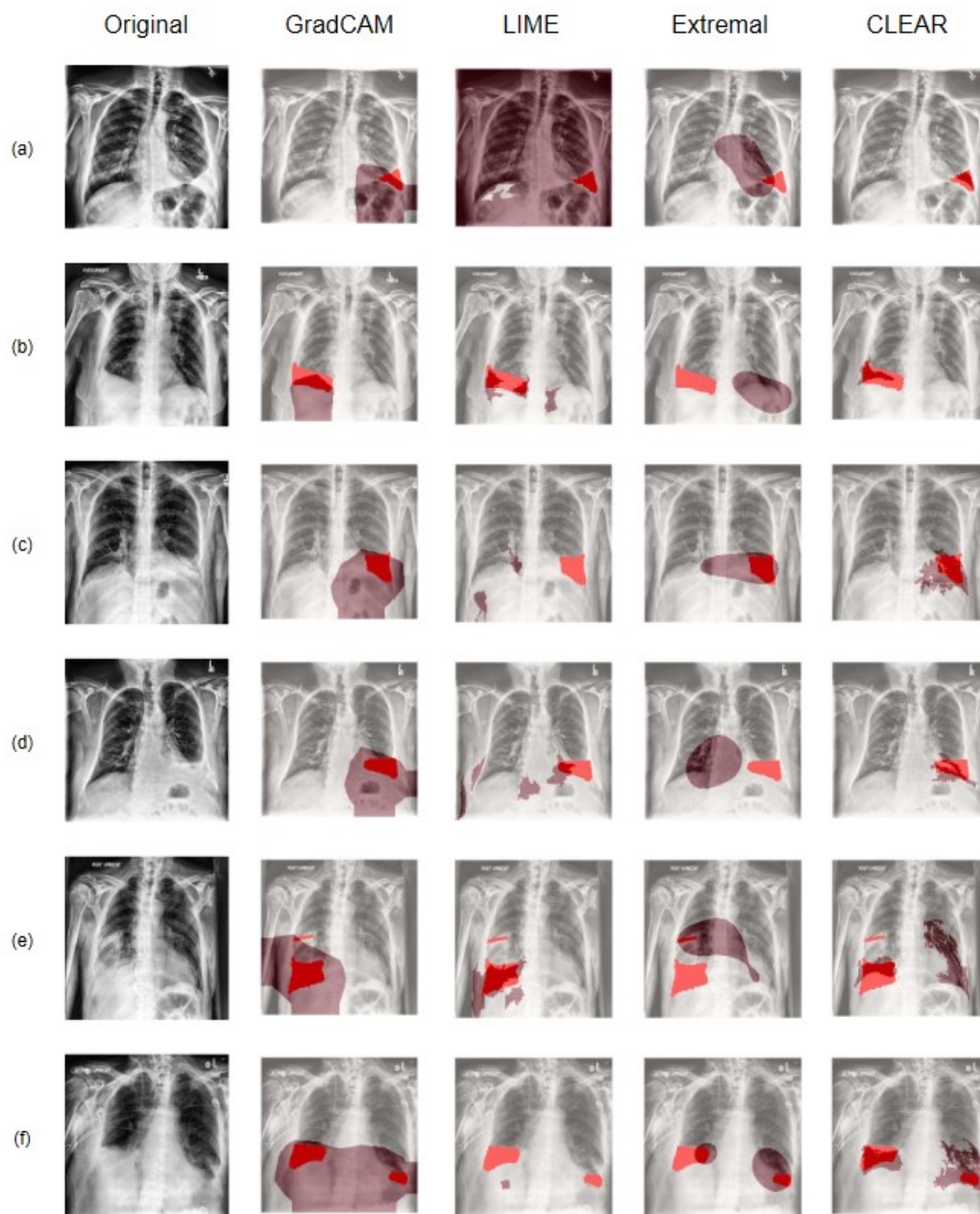


Figure 12: Representative comparative examples of the identified important segments of a VGG16-based image classification model (Val Acc: 97.5%) for pleural effusion using (i) CLEAR *Image*, (ii) Grad-CAM, (iii) Extremal Perturbation and (iv) LIME.



## B Generative Adversarial Network for Image Translation

Generative Adversarial Network (GAN) has been applied as a complementary deep learning tool for synthetic contrastive image generation. This is particularly valuable in the applied use case in medical images where contrasting healthy x-ray images were not available. The following sections will highlight the GAN architecture and the hyperparameters used and present some representative output generated for each use case.

### B.1 DeScarGAN and Parameters

The DeScarGAN architecture was adopted for the synthetic dataset in Section 5.1. 80% of the dataset (4000 images) was used for GAN training and 20% of the dataset (1000 images) was used for validation. A total of 2,500 epochs was run and the best epoch was selected on visual quality. Additional 100 images were generated as an out-of-sample test dataset. Adam optimizer was used with  $\beta_1 = 0.5$ ,  $\beta_2=0.999$ . An initial learning rate of  $10^{-4}$  was used and stepped down to a final learning rate of  $10^{-6}$ . Default hyperparameters for loss functions were used to mimic a similar investigation from the original author as shown below in Table 1:

Loss Term	Weight Value
Adversarial Loss:	$\lambda_{adv,g} = 1$ (Generator) $\lambda_{adv,d} = 20$ (Discriminator)
Gradient Penalty Loss:	$\lambda_{gp} = 10$
Identity Loss:	$\lambda_{id} = 50$
Reconstruction Loss:	$\lambda_{rec} = 50$
Classification Loss:	$\lambda_{cls,g} = 1$ (Generator) $\lambda_{cls,d} = 5$ (Discriminator)

Table 1: Default Loss Function Hyperparameters used in DeScarGAN

### B.2 StarGAN-V2 and Parameters

StarGAN-V2 [5] has been adopted in this work as a state-of-art GAN network for image translation. Within this work, it has provided the necessary contrastive images for the CheXpert dataset. Default hyperparameters were maintained while notable loss weights are highlighted in Table 2. Adam optimizer was used with  $\beta_1 = 0$ ,  $\beta_2=0.99$ . A total of 50,000 epochs was run for the CheXpert dataset. The style encoding is referenced to the input image for the translation to the targeted class. This aids in maintaining the general features of the images compared to the original. As StarGAN-V2 [5] does not constrain its generation to a localised region (e.g. lungs), a post-processing of segmentation and blending was implemented for the CheXpert dataset. Segmentation of the lung region is based on a pre-trained model with a U-Net architecture. The segmentation mask is subsequently used to guide the replacement of pixels within the lung region from the GAN generated healthy image onto the original diseased image. Gaussian Blur is applied to minimise the edge effect during the blending process. This post-processing step aids in restricting the feature identification space within the lungs and reducing the computational cost for locating the counterfactuals.

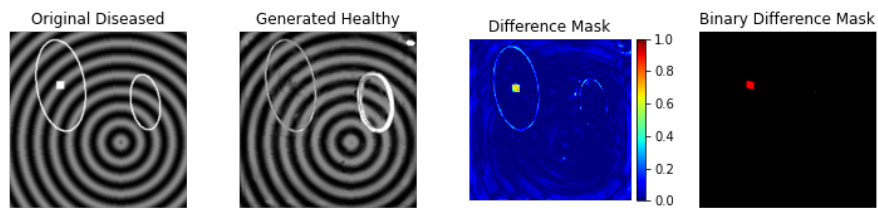
Loss Term	Weight Value
Style Reconstruction Loss:	$\lambda_{sty} = 1$
Style Diversification Loss:	$\lambda_{ds} = 1$
Cyclic Loss:	$\lambda_{cyc} = 1$

Table 2: Default Loss Function Hyperparameters used in StarGANv2 [5]

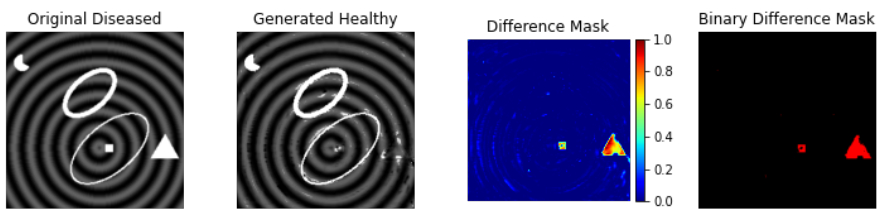
### B.3 Representative Examples for each Use Case

As shown in Figure 13, DeScarGan is capable of identifying pathological objects (e.g. triangles, squares, the thickness of ellipse etc.). Most of these objects are also successfully removed during image generation. Some occasional artefacts remain where partial generation (of the thickened ellipse or other shapes) are found. This is expected without a thorough fine-tuning to optimise the GAN performance. This, however, provides a realistic evaluation of using any publicly available pre-trained GAN for the generation of synthetic counterfactual images needed in the proposed framework.

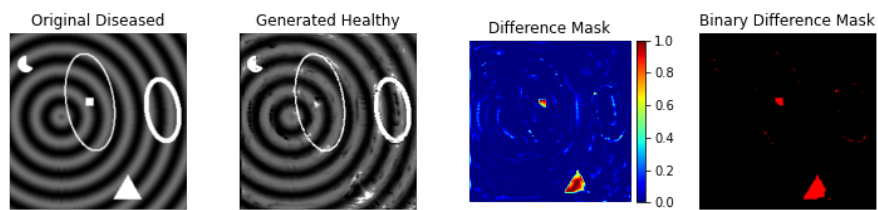
Figure 14 exhibits some representative samples of the final output from the post-processing for the CheXpert dataset. These examples have demonstrated the selected StarGANv2 [5] to be capable of producing high quality X-ray images, and the post-processing segmentation allows lung-specific changes to be altered within the original image. The anatomical structure (e.g. shape & positioning of the rib cage) and other details (e.g. supporting device and wiring) are significantly retained. These blended images will form the source of segment extractions described in the main paper.



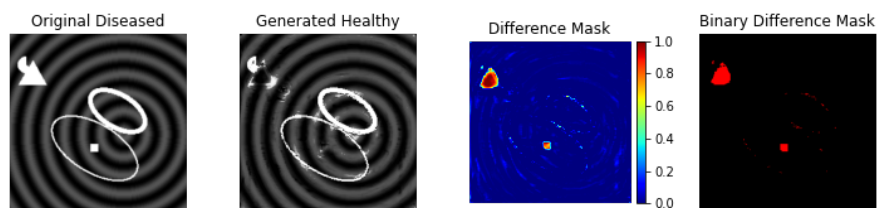
(a)



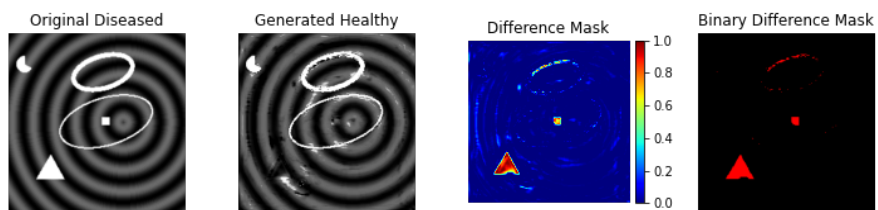
(b)



(c)

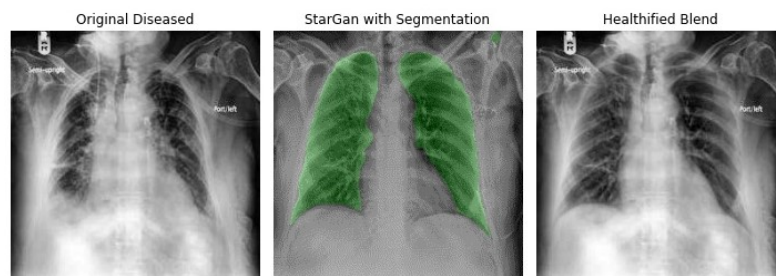


(d)

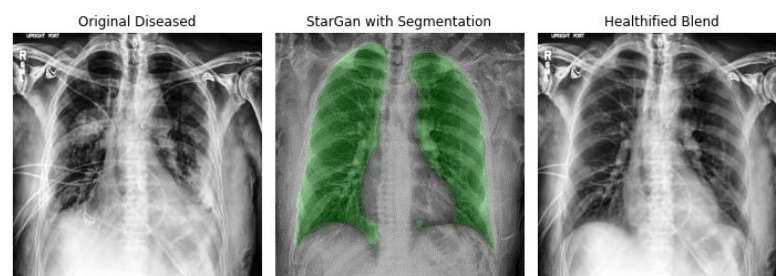


(e)

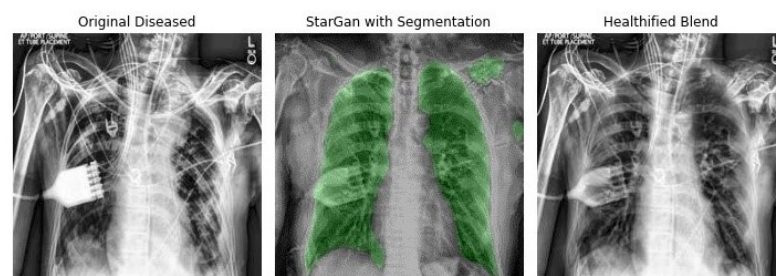
Figure 13: Representative samples of synthetic healthy images with corresponding difference masks. It has successfully identified 'pathological' shapes while ignoring the irrelevant pie.



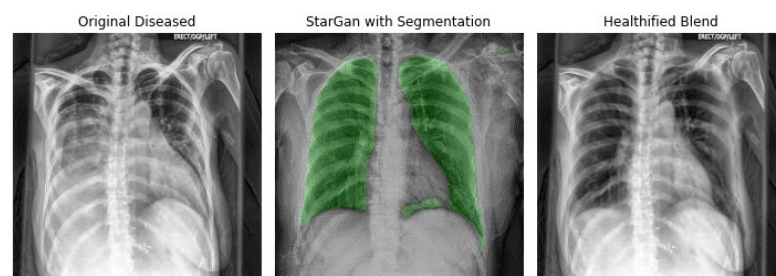
(a)



(b)



(c)



(d)

Figure 14: Representative examples of generated images using StarGANv2 [5]. **Left:** Original diseased. **Middle:** Generated image with post lung segmentation in Green. **Right:** Blended images as Healthy counterfactuals